catalysts

MDPI

*Article*

# $CO_2$ Hydrogenation to Renewable Methane on Ni/Ru Modified ZSM-5 Zeolites: The Role of the Preparation Procedure

**Margarita Popova [1,*], Manuela Oykova [1], Momtchil Dimitrov [1], Daniela Karashanova [2], Daniela Kovacheva [3], Genoveva Atanasova [3] and Ágnes Szegedi [4]**

[1] Institute of Organic Chemistry with Centre of Phytochemistry, Bulgarian Academy of Sciences, 1113 Sofia, Bulgaria
[2] Institute of Optical Materials and Technologies, Bulgarian Academy of Sciences, 1113 Sofia, Bulgaria
[3] Institute of General and Inorganic Chemistry, Bulgarian Academy of Sciences, 1113 Sofia, Bulgaria
[4] Research Centre for Natural Sciences, Institute of Materials and Environmental Chemistry, Magyar tudosok krt.2., 1117 Budapest, Hungary
* Correspondence: margarita.popova@orgchm.bas.bg

**Abstract:** Mono- and bimetallic Ni- and Ru-modified micro-mesoporous ZSM-5 catalysts were prepared by wet impregnation. The influence of the Ni content, the addition of Ru and the sequence of the modification by two metals on the physicochemical properties of the catalysts were studied. They were characterized by X-ray powder diffraction (XRD), $N_2$ physisorption, temperature-programmed reduction (TPR-TGA), TEM and XPS spectroscopy. Formation of finely dispersed nickel and/or ruthenium oxide species was observed on the external surface and in the pores of zeolite support. It was found that the peculiarity of the used zeolite structure and the modification procedure determine the type of formed metal oxides, their dispersion and reducibility. XPS study revealed that the surface became rich in nickel and poorer in ruthenium for bimetallic catalysts. Ni had higher dispersion in the presence of ruthenium, and TPR investigations also confirmed its facilitated reducibility. The studied catalysts were tested in $CO_2$ hydrogenation to methane. 10Ni5RuZSM-5 material showed the highest activity and high selectivity for methane formation, reaching the equilibrium conversion and 100% selectivity at 400 °C. Stability and reusability of the latter catalyst show that it is appropriate for practical application.

**Keywords:** ZSM-5 zeolite; bifunctional catalysts; renewable methane production; gas phase reaction



**Citation:** Popova, M.; Oykova, M.; Dimitrov, M.; Karashanova, D.; Kovacheva, D.; Atanasova, G.; Szegedi, Á. $CO_2$ Hydrogenation to Renewable Methane on Ni/Ru Modified ZSM-5 Zeolites: The Role of the Preparation Procedure. *Catalysts* **2022**, *12*, 1648. https://doi.org/10.3390/catal12121648

Academic Editor: Wladimir Reschetilowski

Received: 22 November 2022
Accepted: 12 December 2022
Published: 15 December 2022



## 1. Introduction

The ongoing intensive use of conventional fuels is associated with increasing carbon emissions and their serious impact on the climate. The European Green Deal, as part of the EU's long-term strategy, aims to address climate change issues by eliminating net greenhouse gas emissions by 2050, most notably $CO_2$, whose emissions reach a record amount of 420 ppm in 2020 [1]. In recent years, technologies have been developed and industrialized to capture $CO_2$ from outgoing gas streams or directly from the atmosphere, after which it can be utilized via transformation processes to chemical substances and fuels [2]. This can be achieved by carboxylation reactions, where the $CO_2$ molecule is used as a precursor for organic compounds, such as carbonates, acrylates and polymers, or in reduction reactions to produce methane, methanol, synthesis gas, urea or formic acid [3,4]. Moreover, $CO_2$ can be used as a feedstock for the production of fuels, for example, by Fischer–Tropsch synthesis or by hydrogenation in the presence of efficient catalysts [5,6]. The Sabatier–Senderens reduction for the hydrogenation of unsaturated organic molecules into saturated ones over a nickel catalyst, later developed to the Fischer–Tropsch synthesis to obtain liquid fuels from coal and natural gas, is today the basis of power-to-gas technologies, based on the integration of the electrochemical production of hydrogen by electrolysis of water by using energy from renewable energy sources and

its further application for hydrogenation of $CO_2$ captured from flue gases from thermal power plants or from industrial plants in order to obtain methane, or the so-called synthetic natural gas (SNG) [7].

The hydrogenation of $CO_2$ to $CH_4$ can proceed as a direct process or through the formation of an intermediate CO, which is hydrogenated at a subsequent step [8,9]. $CO_2$ methanation takes place in the temperature range 200–550 °C and pressures from atmospheric to 80 bars, depending on the type of reactor and catalyst used. A high degree of conversion of about 90% was found at 300 °C over a nickel catalyst at a pressure of 1 atm. and mole ratios of $CO_2/H_2 = 1/4$ and $CO_2/H_2 = 1/5$ [10]. Hydrogenation of $CO_2$ at low temperature extends the life of catalysts as it prevents sintering, agglomeration and deactivation by carbon deposition. The design of the reactor and the structuring of the catalyst are critical to achieve thermal control over the process. Various approaches have been investigated to control and lower the temperature in the reactor-recirculation of part of the outgoing gas flow and cooling of the product gas, isothermal regime of the reactor, which is realized in cooled reactors, where the heat from the reaction zone is brought out to a cooling medium, adiabatic mode for several series-connected fixed-bed reactors with the application of intermediate gas cooling stages or by stepwise addition of reaction mixture [11]. With each of these approaches, difficulties arise related to high thermal stress on the catalyst, occurrence of local overheating zones in the catalytic layer and unwanted energy losses during cooling. Better thermal process control efficiency is expected for the 3D structured catalysts due to the improved packing hydrodynamics. Noble metals (Rh, Ru, Pd, Pt) have been studied as catalysts for the $CO_2$ methanation reaction, due to their high catalytic activity, but from the point of view of the industrialization of this process, of greater interest are the transition metals (Ni, Co, Cu, Fe) due to their affordable price [12]. In the study of the catalytic activity of various catalysts on the hydrogenation of the C-O bond, the following order of activity was established [13]: Rh > Ru > Pd > Pt > Ni > Co >> Cu. The catalytic phase is usually 1–5 wt.% for noble metals and 5–20 wt.% for transition metals. Ni and Ru are extremely selective to produce methane, but due to its high cost, Ru is not of interest despite its highest activity in the methanation reaction. The metals Pd, Pt, Rh, Mo, Re and Au simultaneously catalyze the production of $CH_4$, $CH_3OH$ and CO. Preferred catalysts should be characterized with high selectivity to methane over other hydrocarbons, high activity, stability, lifetime and low cost. Currently, the most promising are catalysts based on nickel (Ni) on supports of: $Al_2O_3$, MCM, SBA-15, $ZrO_2$, $CeO_2$, zeolites. At the same time, catalytic supports have to provide maximum surface area, favorable hydrodynamics, high dispersion of catalytic centers, stability, mechanical strength and thermal resistance [14,15]. Catalytic supports also influence the selectivity and activity of the entire system in the methanation process. Potential candidates for large-scale applications are the Ni/mesoporous $SiO_2$ and $Ni/Al_2O_3$ catalytic systems.

In this study, template-free micro-mesoporous ZSM-5 zeolite was synthesized and modified with Ni and/or Ru. The obtained catalysts were thoroughly characterized and investigated in the $CO_2$ hydrogenation to renewable methane.

## 2. Results and Discussion

### *2.1. Physico-Chemical Properties*

XRD patterns of the parent and metal modified catalysts are shown in Figure 1. Typical crystalline reflections of MFI structure can be observed, besides characteristic peaks of NiO and $RuO_2$ with different intensities. ZSM-5 has a large orthorhombic unit cell with dimensions a = 20.07 Å, b = 19.92 Å and c = 13.42 Å, cell volume 5365.24 $Å^3$ and the non-marked peaks in XRD patterns belong to its structure. The well-crystallized structure of the modified zeolite materials indicate that the impregnation treatment did not create any substantial harm to it. Crystallite sizes of metal oxides are presented in Table 1.

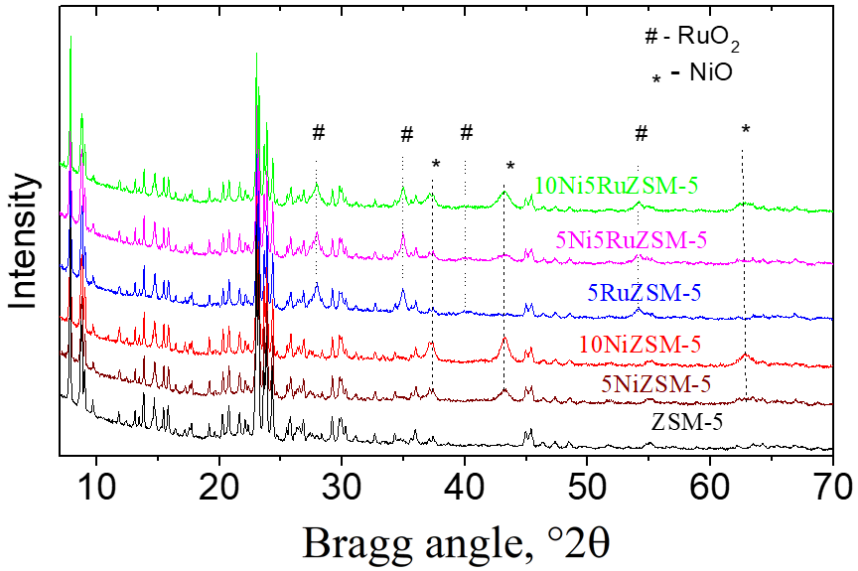


**Figure 1.** X-ray powder diffraction patterns of the initial, and the Ni- and Ru-modified varieties of ZSM-5 catalysts.

**Table 1.** Physico-chemical properties of the studied catalysts.

| Sample | Phase Composition | Cell Parameters, Å | Crystallite Size, nm |
|---|---|---|---|
| 10NiZSM-5 | NiO (Fm-3m) | 4.1815 (7) | 16 |
| Spent 10NiZSM-5 | Ni (Fm-3m) | 3.5241 (4) | 33 |
| 5NiZSM-5 | NiO (Fm-3m) | 4.184 (2) | 13 |
| Spent 5NiZSM-5 | Ni (Fm-3m) | 3.534 (1) | 15 |
| 5RuZSM-5 | $RuO_2$ ($P4_2/mnm$) | 4.511 (1)<br>3.114 (1) | 19 |
| Spent 5RuZSM-5 | Ru ($P6_3/mmc$) | 2.7098 (8)<br>4.285 (2) | 19 |
| 5Ni5RuZSM-5 | NiO (Fm-3m)<br>$RuO_2$ ($P4_2/mnm$) | 4.186 (3)<br>4.511 (1)<br>3.112 (1) | 9<br>21 |
| Spent 5Ni5RuZSM-5 | Ni (Fm-3m)<br>Ru ($P6_3/mmc$) | 3.533 (2)<br>2.699 (2)<br>4.271 (6) | 14<br>9 |
| 10Ni5RuZSM-5 | NiO (Fm-3m)<br>$RuO_2$ ($P4_2/mnm$) | 4.186 (1)<br>4.514 (1)<br>3.110 (1) | 10<br>21 |
| Spent 10Ni5RuZSM-5 | Ni (Fm-3m)<br>Ru ($P6_3/mmc$) | 3.5318 (9)<br>2.696 (4)<br>4.26 (1) | 19<br>7 |

NiO is dispersed relatively finely in the monometallic sample. The crystallite size is 13 nm for 5NiZSM-5 and by increasing the amount of nickel, only a small increase in crystallite size is observed (16 nm). Modification with ruthenium resulted in the formation of 19 nm $RuO_2$ particles on the external surface of the ZSM-5 phase. In bimetallic preparations, the crystallite size of ruthenium oxide did not change, however, that of Ni significantly decreased to 9–10 nm. It seems that the presence of ruthenium favors the formation of smaller NiO particles. Even with double nickel content, the NiO crystallite size did not increase. It is highly probable, based on our former study [16], that a part of metal ions was incorporated into the lattice cationic positions of zeolite.

In Figure 2, nitrogen physisorption isotherms of the initial ZSM-5 zeolite and metal-containing varieties are presented. The corresponding calculated parameters are listed in Table 1. The isotherms are a mixture of type II and IV characteristics for zeolitic materials containing micro- and mesopores. The hysteresis loop is of the H3 type, meaning that the pore size of mesopores shows a wide distribution. Formation of mesopores in zeolites is advantageous from the enhanced mass transfer point of view. Interaction of the support with the modifying metal oxides can also be favored by mesopores, by confining metal/metal oxide nanoparticles and preventing their agglomeration.

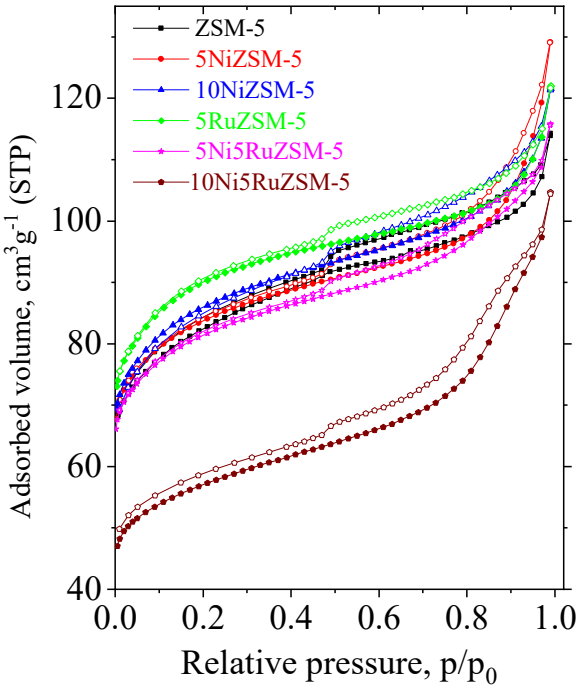


**Figure 2.** Nitrogen adsorption/desorption isotherms of ZSM-5 and the Ni- and Ru-modified ZSM-5 zeolites.

The impregnation procedure does not result in a decrease of the specific surface area of the modified ZSM-5 zeolite, with exception of 10Ni5RuZSM-5, most probably because of the deposition of metal particles on the external surface of the nanosized ZSM-5 blocking part of its micropores (Table 2). Additionally, we can also assume the formation of particles located in the zeolite pores of the latter sample.

**Table 2.** Textural properties of the studied catalysts.

| Samples | SSA [1] ($m^2/g$) | PV [2] ($cm^3/g$) | Micropore Vol. [3] ($cm^3/g$) | Micropore Surf. Area [3] ($m^2/g$) |
|---|---|---|---|---|
| ZSM-5 | 307 | 0.177 | 0.095 | 231 |
| 5NiZSM-5 | 315 | 0.200 | 0.105 | 256 |
| 10NiZSM-5 | 322 | 0.189 | 0.107 | 261 |
| 5RuZSM-5 | 337 | 0.189 | 0.116 | 282 |
| 5Ni5RuZSM-5 | 306 | 0.180 | 0.103 | 250 |
| 10Ni5RuZSM-5 | 215 | 0.162 | 0.065 | 161 |

[1] Specific surface area calculated by the BET method; [2] Total pore volume calculated by the Gurvitch method; [3] Calculated by t-plot method.

TPR-DTG profiles of the nickel and ruthenium-modified mono- and bimetallic materials are shown in Figure 3. TPR-DTG curves of 5RuZSM-5 samples show reduction peaks with high intensity at 190 °C. 5NiZSM-5 and 10NiZSM-5 samples are characterized by two peaks, at 195–205 °C with lower intensity and a higher one between 325–360 °C. The

increase of Ni content leads to the shift of the reduction temperature to higher values for both peaks. The two steps can probably be related to the reduction of NiO particles with different dispersion on the external surface of the zeolite [17]. The bimetallic NiRu-modified samples are presented in Figure 3B.

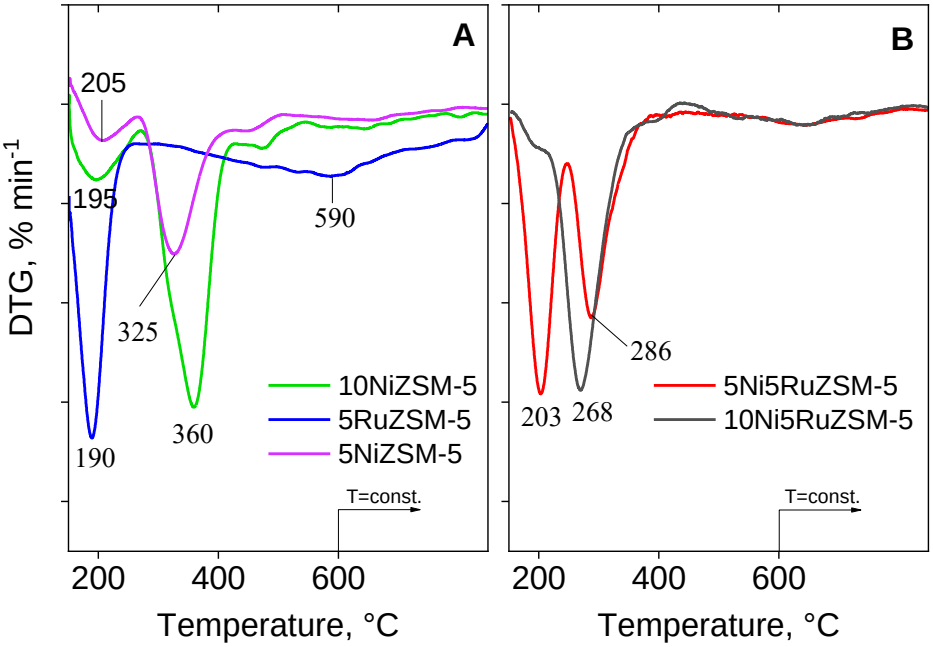


**Figure 3.** TPR-DTG profiles of the Ni- and Ru-modified monometallic (**A**) and bimetallic (**B**) ZSM-5 zeolites.

Two reduction peaks are registered for the 5Ni5RuZSM-5 catalyst, at 203 °C and at 286 °C. However, TPR data for 10Ni5RuZSM-5 is characterized by one broader peak with a maximum at 268 °C. It is obvious that Ru has a beneficial effect on the reducibility of NiO in both NiRuZSM-5 samples, by lowering the reduction temperature.

Bright Field (BF) TEM images, presented in Figure 4a,c,e, reveal the morphology of the studied samples. Small particles with sizes around 10 nm are visualized in the monometallic Ni-containing catalyst, which is in accordance with the results of XRD analysis. These particles, even very tiny, are well crystallized and generate a good polycrystalline Selected Area Electron Diffraction (SAED) pattern (Figure 4b) consisting of reflexes of NiO (cubic, a = 4.16840 A, COD #96-101-0094). Specific elongated and well faceted crystalline particles are found in the Ru-containing monometallic sample. Almost all reflexes registered in the SAED pattern (Figure 4d) correspond to these of $RuO_2$ ($RuO_2$ tetragonal, a = 4.49680 A, c = 3.10490 A, COD #96-100-0059) and one is specific to ZMS-5 (MFI zeolite, orthorhombic, a = 20.50800 A, b = 20.14400 A, c = 13.46500 A, COD #96-154-8623). In the bimetallic 10Ni5RuZSM-5 sample, the BF TEM image (Figure 4e) reveals the presence of the tiny particles, typical for the 10NiZSM-5 catalyst (highlighted in the circle) and large and well faceted plates, attributed to the zeolite substrate. Elongated crystalline particles, visualized in the 5RuZSM-5 catalyst, are not found here. However, the co-existence of the three phases: NiO, $RuO_2$ and zeolite in this sample is proved by the SAED pattern.

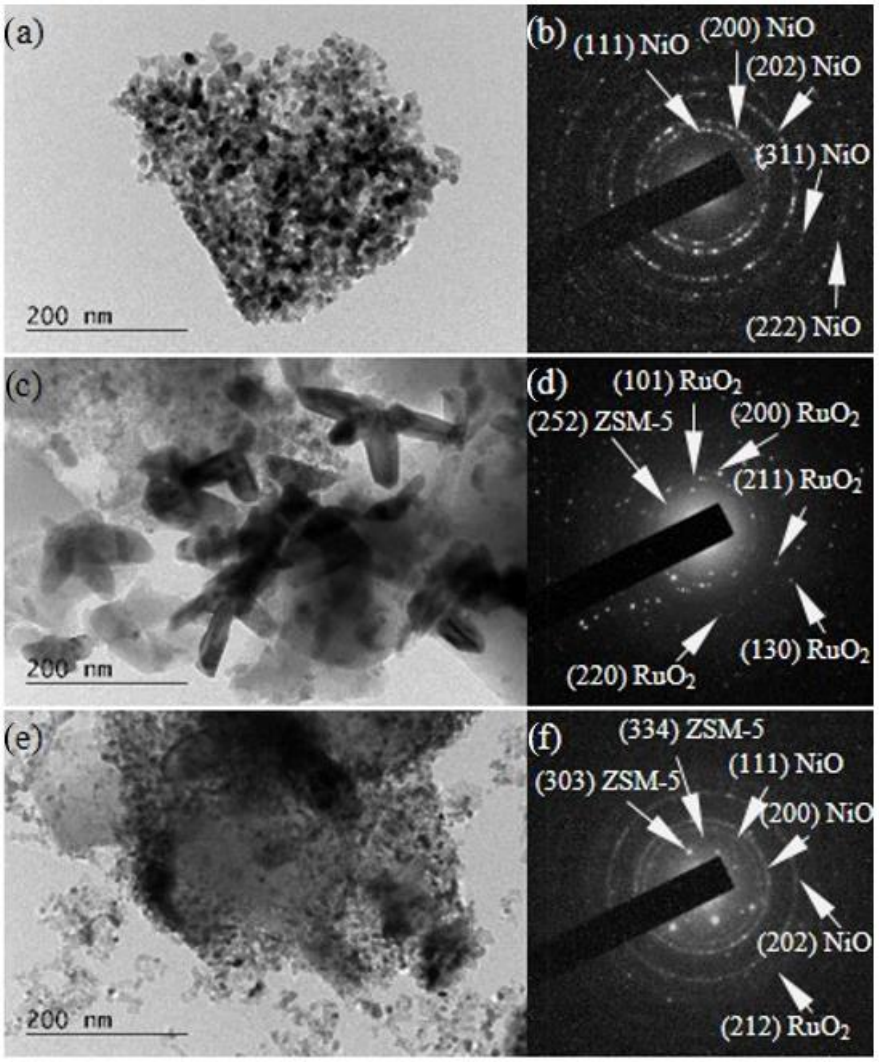


**Figure 4.** TEM images of 10NiZSM-5 (**a**), 5RuZSM-5 (**c**) and 5Ru10NiZSM-5 (**e**) zeolites and SAED patterns of 10NiZSM-5 (**b**), 5RuZSM-5 (**d**) and 5Ru10NiZSM-5 (**f**).

The surface chemical composition was calculated from the ratio of the corresponding intensities of O 1s, Si 2p, Al 2p, Ni $2p_{3/2}$ and Ru 3d photoelectron peaks corrected by the Scofield's photoionization cross sections and the obtained data are presented in Table 3. The nickel content in 10Ni5RuZSM-5 is exposed to the zeolite surface and can participate in the reaction as active sites whereas only a small part of Ru is accessible for the reactant molecules. The surface nickel content is higher on the bimetallic sample and ruthenium is lower compared to monometallic varieties. The results are in good agreement with TPR data, showing easier reduction of nickel in bimetallic preparations, which can be due to the high density of nickel nanoparticles on the surface.

### *2.2. Catalytic Activity for $CO_2$ Hydrogenation to Methane*

Zeolite catalysts were studied in hydrogenation of $CO_2$ to methane (Figure 6). Activity was increased with increasing temperature for all samples, until equilibrium was achieved at 400 °C only for 10Ni5RuZSM-5.

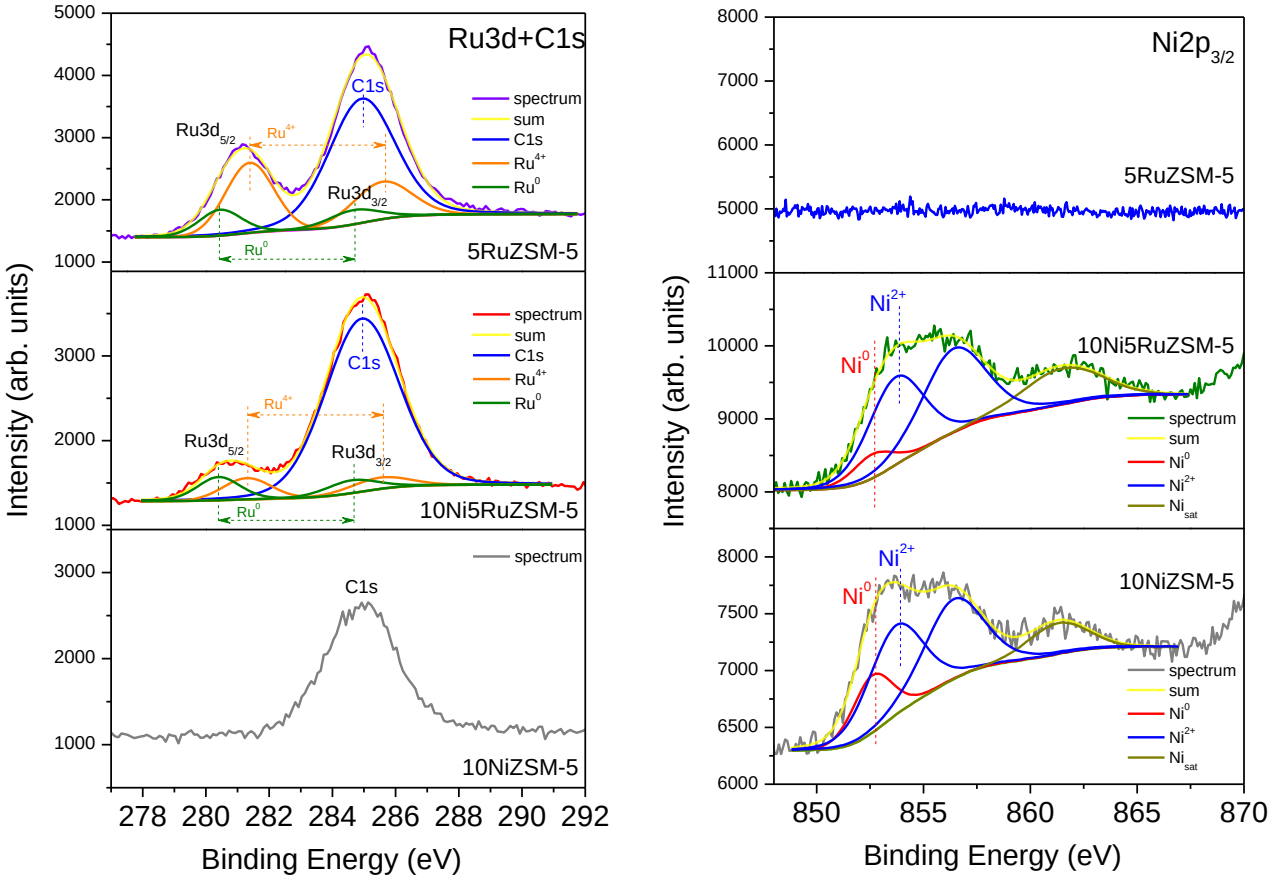


**Figure 5.** Ru3d and Ni2p$_{3/2}$ XPS spectra of the reduced 10NiZSM-5, 5RuZSM-5 and 10Ni5RuZSM-5 zeolites.

**Table 3.** Surface chemical composition of the parent catalysts.

| Samples | O (at.%) | Si (at.%) | Ni (at.%) | Al (at.%) | Ru (at.%) |
|---|---|---|---|---|---|
| 10NiZSM-5 | 58.5 | 32.2 | 3.9 | 5.4 | - |
| 5RuZSM-5 | 59.5 | 35.8 | - | 2.7 | 2.0 |
| 10Ni5RuZSM-5 | 54.0 | 29.1 | 6.8 | 8.9 | 1.2 |

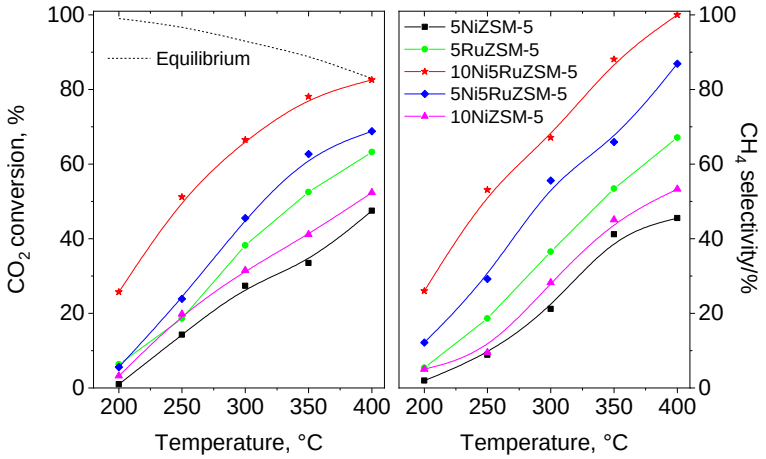


**Figure 6.** Catalytic activity vs. temperature for the studied catalysts ($H_2$:$CO_2$ = 4:1; GHSV = 30,000 mL $g_{cat}^{-1}$ $h^{-1}$).

It can be observed that two times higher Ni content leads only to a slight improvement of catalytic activity. This is in connection with dispersion of metallic nickel on the catalysts. A higher amount of metal makes agglomeration of metallic nanoparticles more probable, decreasing the accessible number of active sites on the surface. As could be expected, Ru-containing samples are more active than Ni-containing ones even with higher nickel content. A higher temperature is needed for transition metal containing catalysts to achieve the same activity. Bimetallic samples show higher catalytic activity than monometallic ones. The 10Ni5RuZSM-5 catalyst performs much better than any other catalyst, even 5Ni5RuZSM-5 material, reaching equilibrium at 400 °C. The selectivity to methane is following the same trend as activity, which is indicative of a typical stepwise reaction in which CO was an intermediate in the process of $CH_4$ formation. The 100% selectivity can be reached only with the most active catalyst, 10Ni5RuZSM-5, at 400 °C. Comparing the selectivity of the different catalysts at the same activity, around 25% (Table 4), it can be seen that monometallic catalysts show somewhat lower values, and bimetallic create a group with higher, but rather similar selectivity. Based on the literature, the Ru loading (up to 5 wt.%) favors the $CH_4$ formation, which is due to the improved dissociation of $H_2$ and hence, increased $H_2$ adsorption capacity [20]. The latter could explain the higher selectivity to $CH_4$ on monometallic 5RuZSM-5 and bimetallic 5Ni5RuZSM-5 and 10Ni5RuZSM-5 catalysts in comparison to Ni-containing ones.

**Table 4.** $CH_4$ selectivity of the catalysts at similar catalytic activity (25%).

| Sample | $CH_4$ Selectivity, % |
|---|---|
| 5NiZSM-5 | 20 |
| 10NiZSM-5 | 19 |
| 5RuZSM-5 | 25 |
| 5Ni5RuZSM-5 | 29 |
| 10Ni5RuZSM-5 | 31 |

$CO_2$ conversion to methane is a consecutive reaction, the first step is the reduction of $CO_2$ to CO (adsorbed) on the surface of metal(s) followed by hydrogenation to $CH_4$ [21,22]. However, according to Kwak et al. [20], direct CO formation on a different active center cannot be excluded.

When small metal nanoparticles (around 10 nm) are present, the initially formed CO can easily be hydrogenated to $CH_4$ on these particles [23]. It has been previously observed that both Ni and Ru can adsorb $CO_2$ [24]. In our case, the zeolite support favors the adsorption of $CO_2$, promoting a better metal–support interaction. Moreover, the addition of Ru facilitates the reducibility of the Ni species, thus favoring the formation of smaller nanoparticles and diminishing their aggregation under reaction conditions. The high density of the Ni and Ru particles in our bimetallic catalysts helps the activation of $CO_2$ and CO on the metallic sites [25]. The use of zeolite support favors the formation of small NiO crystallite and also improved the reducibility and the stability of the metallic particles under reaction conditions. Additionally, the procedure for metals deposition, including as a first step ruthenium deposition followed by nickel deposition, allows obtaining smaller NiO crystallites in bimetallic samples. It is well known that the catalytic activity increases up to a Ni loading of 10 wt.%, above which a decrease in catalytic activity is observed due to catalysts sintering and non-uniform metal distribution. The addition of Ru to the Ni-based catalyst decreased NiO particle size and improved the $H_2$ dissociative adsorption capacity. Similar NiO nano crystallites were detected for both bimetallic samples despite a two times higher amount of Ni in 10Ni5RuZSM-5. The differences between both Ni-containing catalysts could justify the different improvements in the methanation reaction produced by Ru addition. Besides, a higher XPS surface proportion of Ni (6.8 at.%) in 10Ni5RuZSM-5 in comparison with Ni in monometallic 10NiZSM-5 (3.9 at.%) was observed.

Stability of the best performing catalyst was checked at 400 °C for 6 h. The activity loss was below 5%. Moreover, regeneration in air and repeated reduction in hydrogen

at 400 °C did not change the activity of the catalyst. In contrast, monometallic variety with 10% Ni showed a 40% decrease during the same period. In order to explain the registered changes in the catalytic activity, XRD measurements of the spent 10Ni5RuZSM-5 and 10NiZSM-5 catalysts were performed. The results show the increase of the $Ni^0$ nanoparticles in 10NiZSM-5, whereas a small increase of the Ni particles and decrease of Ru particles sizes in 10Ni5RuZSM-5 were detected. The redispersion of Ru could be a reason for the good catalytic stability of the bimetallic 10Ni5RuZSM-5 catalyst. The formation of carbon deposits on the surface of the spent catalysts was determined by TG analysis. The results show 4.0 wt.% coke formation for the 10NiZSM-5 catalysts and 3.7 wt.% for the 10Ni5RuZSM-5 catalysts. It is a well-known phenomenon that the presence of noble metals reduced the tendency of coke formation [23].

Considering the high activity of the bimetallic 10Ni5RuZSM-5 sample, it is important to compare its activity with other types of catalysts used for $CO_2$ methanation [18,26–28] (Table 5). Among noble metal-containing catalysts, Ni-Ru/$Al_2O_3$ showed the best performance for $CO_2$ hydrogenation to $CH_4$ [18], but the reaction is carried out at lower GHSV (GHSV = 9000 mL $g_{cat}^{-1}$ $h^{-1}$). However, the information about the catalyst stability is scarce in the cited literature but the stabilization of highly dispersed metal nanoparticles is difficult but very important to obtain for practical application.

**Table 5.** Comparison of the catalytic activity of the supported catalysts from the literature studied in this reaction.

| Catalysts | Reaction Conditions | Catalytic Activity, % | Reference |
|---|---|---|---|
| $Ni/SiO_2$ | T = 350 °C; 5 wt.% Ni; GHSV = 15,000 mL $g_{cat}^{-1}$ $h^{-1}$ | X = 64.7%; $S_{CH4}$ = 97.5% | [25] |
| Ni-Rh/$Al_2O_3$ | T = 400 °C; 3.1 wt.% Ni; 0.5 wt.% Rh; GHSV = 60,000 mL $g_{cat}^{-1}$ $h^{-1}$ | X = 65%; $S_{CH4}$ = 95% | [26] |
| Ni-Co/$Al_2O_3$ | T = 350 °C; 10 wt.% Ni; 10 wt.% Co; GHSV = 133,000 mL $g_{cat}^{-1}$ $h^{-1}$ | X = 61.5%; $S_{CH4}$ = 95% | [27] |
| Ni-Ru/$Al_2O_3$ | T = 400 °C; 10 wt.% Ni; 1 wt.% Ru; GHSV = 9000 mL $g_{cat}^{-1}$ $h^{-1}$ | X = 82%; $S_{CH4}$ = 100% | [18] |
| Ru-Ni/CeZr | T = 400 °C; 15 wt.% Ni; 1 wt.% Ru; GHSV = 24,000 mL $g_{cat}^{-1}$ $h^{-1}$ | X = 62%; $S_{CH4}$ = 90% | [28] |
| Ni-Ru/ZSM-5 | T = 400 °C; 10 wt.% Ni; 5 wt.% Ru; GHSV = 30,000 mL $g_{cat}^{-1}$ $h^{-1}$ | X = 82%; $S_{CH4}$ = 100% | This work |

Summarizing the catalytic activity results, it was found that bimetallic catalysts have higher activity and selectivity to methane formation, and the catalyst stability was also significantly improved. We can point out that the higher amount of non-noble transition metal (nickel) in the bimetallic catalysts has a positive effect in both activity and stability in the studied reaction.

## 3. Experimental

### *3.1. Materials*

The reagents used for the preparation of nanosized ZSM-5 zeolite are sodium hydroxide (NaOH, analytical grade, Aldrich, St. Louis, MO, USA), $NaAlO_2$ (Aldrich), aluminum sulphate ($Al_2(SO_4)_3 \cdot 18H_2O$, analytical grade, Aldrich), sodium carbonate ($Na_2CO_3$, analytical grade, Aldrich), tetraethyl orthosilicalite (TEOS, analytical grade, Aldrich), silicon(IV)oxide, 40% in $H_2O$ colloidal dispersion ($SiO_2$, analytical grade, Aldrich) and $H_2SO_4$ (Aldrich). $Ni(NO_3)_2 \cdot 6H_2O$ and $RuCl_3$ were purchased from Aldrich.

### *3.2. Preparation of Seed Crystals*

ZSM-5 seed crystals were prepared with the molar ratio of $12Na_2O{:}80SiO_2{:}2Al_2O_3{:}2500H_2O$. The synthesis procedure was as follows: NaOH and $NaAlO_2$ were dissolved in distilled water, followed by the addition of silica sol dropwise with stirring for 5 h. Then, the mixture sol was transferred to a Teflon-lined autoclave and crystallized at 220 °C for 4 h. The products were separated by centrifugation, washed with distilled water for three times and dried at 80 °C for 12 h.

### 3.3. Synthesis of ZSM-5 Zeolite

The synthesis of ZSM-5 was carried out by template-free synthesis with some modifications [29]. In brief, $NaAlO_2$ and NaOH were mixed, and the colloidal silica was added to the solution under continuous stirring for a few minutes. Then, 1 wt.% of the seed suspension was added to the gel mixture. $Al_2(SO_4)_3 \cdot 18H_2O$, and 15 mL deionized water were added and stirred at room temperature for 4 h to prepare a mixed gel. Finally, the final gel was transferred to a Teflon-lined autoclave and hydrothermally crystallized for 24 h at 165 °C. After that, ZSM-5 powder was filtered, washed with water and dried at 100 °C overnight.

### 3.4. Modification with Ni or/and Ru Nanoparticles of ZSM-5 Zeolite

An impregnation technique with nickel and ruthenium salts was applied for loading of 5 wt.% and 10 wt.% metals, respectively. The supports were heated at 160 °C for 2 h before the impregnation procedure. A monometallic Ni-modified ZSM-5 sample was prepared by the following procedure: 130.3 mg $Ni(NO_3)_2 \cdot 6H_2O$ was dissolved in 5 mL ethanol and added to 500 mg ZSM-5 support by stirring for 10 min. The sample was then dried at 80 °C for 18 h and calcined at 450 °C for 3 h at a rate of 1 °C/min.

The sample was denoted as 10Ni/ZSM-5. A monometallic 10Ni-modified ZSM-5 sample was prepared by dissolving 275 mg $Ni(NO_3)_2 \cdot 6H_2O$ in 5 mL ethanol and subsequently added to 500 mg ZSM-5, which was heated at 160 °C for 2 h before the impregnation procedure. The sample was supported by stirring for 10 min. After this procedure, the sample was dried at 80 °C for 18 h and calcined at 450 °C for 3 h at a rate of 1 °C/min.

The monometallic Ru-modified ZSM-5 sample was prepared by dissolving 160.9 mg $RuCl_3$ in 40 mL water and subsequently adding the solution to 1500 mg ZSM-5 support by stirring at room temperature for 12 h. The solvent was removed in a rotary vacuum evaporator at 40 °C. The sample was then dried at 110 °C for 12 h and calcined at 450 °C for 3 h at a rate of 1 °C/min. The sample was denoted as 5RuZSM-5.

The bimetallic 5 wt.% Ru- and 5 wt.% Ni-modified ZSM-5 sample was prepared by the following procedure: A solution of 130.31 mg $Ni(NO_3)_2 \cdot 6H_2O$ in 4 mL ethanol was added to 500 mg 5RuZSM-5, which was heated at 160 °C for 2 h before the impregnation procedure. The sample was supported by stirring for 10 min. After this procedure, the sample was dried at 80 °C for 18 h. The precursor salt was decomposed in air at 450 °C at a rate of 1 °C /min for 3 h. The sample was denoted as 5Ni5RuZSM-5.

Bimetallic 5 wt.% Ru- and 10 wt.% Ni-modified ZSM-5 samples were prepared by the following procedure: 275 mg $Ni(NO_3)_2 \cdot 6H_2O$ was dissolved in 5 mL ethanol and subsequently added to 500 mg 5RuZSM-5, which was heated at 160 °C for 2 h before the impregnation procedure. The sample was supported by stirring for 10 min. The precursor salt was decomposed in air at 450 °C at a rate of 1 °C/min for 3 h. The sample was denoted as 10Ni5RuZSM-5.

### 3.5. Characterization

Powder X-ray diffraction patterns were collected on a Bruker D8 Advance diffractometer with Cu Kα radiation and a LynxEye detector with a constant step of 0.02° 2θ. For the identification of crystalline phases, the ICDD-PDF2 database (2021) was used. Mean crystallite sizes were determined by the Topas-4.2 software.

The specific surface area, pore volume and size of all samples were determined from $N_2$ physisorption isotherms collected at −196 °C using AUTOSORB iQ-C-MP-AG-AG (Quantachrome Instruments (Anton Paar brand), Ashland, VA, USA). Samples were pretreated at 150 °C under vacuum for 15 h.

The TEM images were taken on JEOL JEM 2100 HRTEM (200 kV, Tokyo, Japan). The samples were suspended in a small amount of analytical grade ethanol and a drop of the suspension was deposited onto a copper grid covered by carbon supporting film and dried at ambient atmosphere.

The temperature-programmed reduction-thermogravimetric analysis (TPR-TGA) investigations were performed by a STA449F5 Jupiter type instrument of NETZSCH Gerätebau GmbH (Selb, Germany). In a typical measurement, 20 mg of sample was placed in a microbalance crucible and heated in a flow of 5 vol.% $H_2$ in Ar (50 $cm^3$/min) up to 500 °C at 5 °C/min and a final hold-up of 1 h. Prior to the TPR experiments, the samples were treated in situ in an air flow (10 °C/min) up to 500 °C, followed by a hold-up of 1 h.

The composition and the chemical properties of the selected samples were analyzed by X-ray photoelectron spectroscopy (XPS). XPS measurements were performed in the UHV chamber of an ESCALAB-Mk II (VG Scientific, Waltham, MA, USA) electron spectrometer with Al $K_{\alpha 1,2}$ radiation (hν = 1486.6 eV). The surface composition was obtained from the ratio of the corresponding intensities of O 1s, Si 2p, Al 2p, Ni $2p_{3/2}$ and Ru 3d photoelectron peaks corrected by the Scofield's photoionization cross sections. The spectra were calibrated according to the Si 2p peak at 103.4 eV.

### *3.6. Catalytic Activity Measurements*

Prior to the catalytic tests, samples were pretreated for 1 h in hydrogen (60 mL/min) up to 673 K. Hydrogenation of methane was studied at an atmospheric pressure using a fixed-bed flow reactor. In the reaction, the 100 mg sample (particle size 0.2–0.8 mm) was tested, diluted with 100 mg glass beads of the same diameter, previously checked to be inactive. The reactor itself was a quartz tube of a 15 mm inner diameter, with the catalyst bed at the middle. A thermocouple was positioned in the catalyst bed for accurate measurement of the catalyst temperature. All gas lines of the apparatus were heated continuously at 383 K in order to minimize reactant and products adsorption on the tube walls. The $CO_2$ reactant was fed in the reactor with a flow rate of 50 mL/min $H_2$, $CO_2$ and $N_2$ (20%) ($H_2/CO_2$ is 4/1) and catalytic tests were carried out in the temperature range 250–400 °C. The reaction steady state was established after 30 min in each temperature. On-line analysis of the reaction products was performed using on NEXIS GC-2030 ATF with a VALCO Plot VPHS-D CFS-PD3053-200 (30 m × 0.53 mm × 20.0 μm).

## 4. Conclusions

A series of Ni- and/or Ru-modified ZSM-5 zeolite catalysts were prepared by the wet impregnation method. The applied Ni content, the addition of Ru as a second metal and the sequence of the modification by two metals are of key importance for the preparation of bimetallic catalysts with appropriate physico-chemical characteristics. Finely dispersed nickel and ruthenium oxide nanoparticles were registered to be formed on the external surface of zeolite by precursor salt decomposition. XPS data reveal that in bimetallic systems, the surface is richer in nickel than in monometallic ones, due to higher dispersion of Ni, enhanced by the presence of ruthenium. However, surface density of ruthenium is lower in bimetallic preparations compared to the monometallic one. In connection with former facts, TPR study confirmed the facilitated reducibility of nickel oxide particles in the presence of noble metal. Among the studied catalysts, 10Ni5RuZSM-5 composition shows the highest activity and high selectivity for methane formation, reaching the equilibrium conversion and 100% selectivity at 400 °C. High stability and good reusability were found for the bimetallic 10Ni5RuZSM-5 catalyst.

**Author Contributions:** Conceptualization, M.P. and M.D.; methodology, M.P., M.D., D.K. (Daniela Karashanova), D.K. (Daniela Kovacheva) and G.A.; formal analysis, M.O., D.K. (Daniela Karashanova), D.K. (Daniela Kovacheva) and G.A.; investigation, M.P., M.D., M.O., Á.S., D.K. (Daniela Karashanova), D.K. (Daniela Kovacheva) and G.A.; data curation, M.O.; writing—original draft preparation, M.P., M.O., M.D., D.K. (Daniela Karashanova), D.K. (Daniela Kovacheva) and G.A.; writing—review and editing, M.P., M.D. and Á.S.; visualization, M.P., Á.S. and M.D.; supervision, M.P.; project administration, M.P.; funding acquisition, M.P. All authors have read and agreed to the published version of the manuscript.

**Funding:** Margarita Popova and Manuela Oykova thank for the financial support of the National Science Found of Bulgaria, grant № КП-06-КОСТ/11/2021. Support of this work in the framework of the bilateral grant agreement between the Bulgarian Academy of Sciences and the Hungarian Academy of Sciences (IC-HU/02/2022–2023, NKM-37/2022) is gratefully acknowledged. Daniela Karashanova thanks for the financial support of Research equipment of Distributed Research Infrastructure IN-FRAMAT, part of Bulgarian National Roadmap for Research Infrastructures, supported by Bulgarian Ministry of Education and Science was used in this investigation.

**Data Availability Statement:** Not applicable.

**Conflicts of Interest:** The authors declare no conflict of interest.

## References

1. Lüthi, D.; Le Floch, M.; Bereiter, B.; Blunier, T.; Barnola, J.-M.; Siegenthaler, U.; Raynaud, D.; Jouzel, J.; Fischer, H.; Kawamura, K.; et al. High-resolution carbon dioxide concentration record 650,000-800,000 years before present. *Nature* **2008**, *453*, 379–382. [CrossRef] [PubMed]
2. Hasan, M.F.; Zantye, M.S.; Kazi, M.-K. Challenges and opportunities in carbon capture, utilization and storage: A process systems engineering perspective. *Comput. Chem. Eng.* **2022**, *166*, 107925. [CrossRef]
3. Styring, P.; Jansen, D.; de Coninck, H.; Armstrong, K. *Carbon Capture and Utilisation in the Green Economy*; Centre for Low Carbon Futures: New York, NY, USA, 2011.
4. Markewitz, P.; Kuckshinrichs, W.; Leitner, W.; Linssen, J.; Zapp, P.; Bongartz, R.; Schreiber, A.; Müller, T.E. Worldwide innovations in the development of carbon capture technologies and the utilization of $CO_2$. *Energy Environ. Sci.* **2012**, *5*, 7281–7305. [CrossRef]
5. Von der Assen, N.; Voll, P.; Peters, M.; Bardow, A. Life cycle assessment of $CO_2$ capture and utilization: A tutorial review. *Chem. Soc. Rev.* **2014**, *43*, 7982–7994. [CrossRef]
6. Lee, W.J.; Li, C.; Prajitno, H.; Yoo, J.; Patel, J.; Yang, Y.; Lim, S. Recent trend in thermal catalytic low temperature $CO_2$ methanation: A critical review. *Catal. Today* **2020**, *368*, 2–19. [CrossRef]
7. Wulf, C.; Linssen, J.; Zapp, P. Power-to-Gas—Concepts, Demonstration, and Prospects. In *Hydrogen Supply Chains*; Elsevier: Amsterdam, The Netherlands, 2018; pp. 309–345.
8. Munnik, P.; Velthoen, M.E.Z.; de Jongh, P.E.; de Jong, K.P.; Gommes, C.J. Nanoparticle Growth in Supported Nickel Catalysts during Methanation Reaction-Larger is Better. *Angew. Chem.* **2014**, *126*, 9647–9651. [CrossRef]
9. Bacariza, M.C.; Graça, I.; Lopes, J.M.; Henriques, C. Tuning Zeolite Properties towards $CO_2$ Methanation: An Overview. *ChemCatChem* **2019**, *11*, 2388–2400. [CrossRef]
10. Sahebdelfar, S.; Takht Ravanchi, M. Carbon dioxide utilization for methane production: A thermodynamic analysis. *J. Pet. Sci. Eng.* **2015**, *134*, 14–22. [CrossRef]
11. Held, M.; Schollenberger, D.; Sauerschell, S.; Bajohr, S.; Kolb, T. Power-to-Gas: $CO_2$ Methanation Concepts for SNG Production at the Engler-Bunte-Institut. *Chem. Ing. Tech.* **2020**, *92*, 595–602. [CrossRef]
12. Frontera, P.; Macario, A.; Ferraro, M.; Antonucci, P. Supported Catalysts for $CO_2$ Methanation: A Review. *Catalysts* **2017**, *7*, 59. [CrossRef]
13. Younas, M.; Loong Kong, L.; Bashir, M.J.K.; Nadeem, H.; Shehzad, A.; Sethupathi, S. Recent Advancements, Fundamental Challenges, and Opportunities in Catalytic Methanation of $CO_2$. *Energy Fuels* **2016**, *30*, 8815–8831. [CrossRef]
14. Guo, X.; Traitangwong, A.; Hu, M.; Zuo, C.; Meeyoo, V.; Peng, Z.; Li, C. Carbon Dioxide Methanation over Nickel-Based Catalysts Supported on Various Mesoporous Material. *Energy Fuels* **2018**, *32*, 3681–3689. [CrossRef]
15. Paviotti, M.; Faroldi, B.; Cornaglia, L. Ni-based catalyst over rice husk-derived silica for the $CO_2$ methanation reaction: Effect of Ru addition. *J. Environ. Chem. Eng.* **2021**, *9*, 105173. [CrossRef]
16. Popova, M.; Szegedi, Á.; Oykova, M.; Lazarova, H.; Koseva, N.; Mihályi, M.R.; Shestakova, P. Selective production of phenol on bifunctional, hierarchical ZSM-5 zeolites. *Molecules* **2021**, *26*, 3576. [CrossRef] [PubMed]
17. Szegedi, Á.; Popova, M.; Mavrodinova, V.; Urbán, M.; Kiricsi, I.; Minchev, C. Synthesis and characterization of Ni-MCM-41 materials with spherical morphology and their catalytic activity in toluene hydrogenation. *Microporous Mesoporous Mater.* **2007**, *99*, 149–158. [CrossRef]
18. Zhen, W.; Li, B.; Lu, G.; Ma, J. Enhancing catalytic activity and stability for $CO_2$ methanation on Ni-Ru/g-$Al_2O_3$ via modulating impregnation sequence and controlling surface active species. *RSC Adv.* **2014**, *4*, 16472–16479. [CrossRef]
19. Biesinger, M.C.; Payne, B.P.; Lau, L.W.M.; Gerson, A.; Smart, R.S.C. X-ray photoelectron spectroscopic chemical state quantification of mixed nickelmetal, oxide and hydroxide systems. *Surf. Interface Anal.* **2009**, *41*, 324–332. [CrossRef]
20. Kwak, J.H.; Kovarik, L.; Szanyi, J. $CO_2$ reduction on supported Ru/Al2O3 catalysts: Cluster size dependence of product selectivity. *ACS Catal.* **2013**, *3*, 2449–2455. [CrossRef]
21. Wu, H.C.; Chang, Y.C.; Wu, J.H.; Lin, J.H.; Lin, I.K.; Chen, C.S. Methanation of $CO_2$ and reverse water gas shift reactions on Ni/$SiO_2$ catalysts: The influence of particle size on selectivity and reaction pathway. *Catal. Sci. Technol.* **2015**, *5*, 4154–4163. [CrossRef]
22. Beuls, A.; Swalus, C.; Jacquemin, M.; Heyen, G.; Karelovic, A.; Ruiz, P. Methanation of $CO_2$: Further insight into the mechanism over Rh/γ-Al2O3 catalyst. *Appl. Catal. B Environ.* **2012**, *113–114*, 2–10. [CrossRef]

23. Le, T.A.; Kim, M.S.; Lee, S.H.; Kim, T.W.; Park, E.D. CO and $CO_2$ methanation over supported Ni catalysts. *Catal. Today* **2016**, *293–294*, 89–96. [CrossRef]
24. Quindimil, A.; De-La-Torre, U.; Pereda-Ayo, B.; Davo-Quinonero, A.; Bailon-García, E.; Lozano-Castello, D.; Gonzalez-Marcos, J.A.; Bueno-Lopez, A.; Gonzalez-Velasco, J.R. Effect of metal loading on the $CO_2$ methanation: A comparison between alumina supported Ni and Ru catalysts. *Catal. Today* **2020**, *356*, 419–432. [CrossRef]
25. Guo, M.; Lu, G. The difference of roles of alkaline-earth metal oxides on silica-supported nickel catalysts for $CO_2$ methanation. *RSC Adv.* **2014**, *4*, 58171–58177. [CrossRef]
26. Mutz, B.; Sprenger, P.; Wang, W.; Wang, D.; Kleist, W.; Grunwaldt, J.-D. Operando Raman spectroscopy on $CO_2$ methanation over alumina-supported Ni, Ni3Fe and NiRh0.1 catalysts: Role of carbon formation as possible deactivation pathway. *Appl. Catal. A Gen.* **2018**, *556*, 160–171. [CrossRef]
27. Alrafei, B.; Polaert, I.; Ledoux, A.; Azzolina-Jury, F. Remarkably stable and efficient Ni and Ni-Co catalysts for $CO_2$ methanation. *Catal. Today* **2020**, *346*, 23–33. [CrossRef]
28. Sache, E.; le Pastor-Perez, L.; Haycock, B.J.; Villora-Pico, J.J.; Sepúlveda-Escribano, A.; Reina, T.R. Switchable catalysts for chemical $CO_2$ recycling: A step forward in the methanation and reverse water–gas shift reactions. *ACS Sustain. Chem. Eng.* **2020**, *8*, 4614–4622. [CrossRef]
29. Ye, T.; Chen, Z.; Chen, Y.; Xie, H.; Zhong, Q.; Qu, H. Green synthesis of ZSM-5 zeolite for selective catalytic reduction of NO via template-free method from tailing residue. *J. Environ. Chem. Eng.* **2022**, *10*, 107766. [CrossRef]